Transmission electron microscopy of the induced damage by argon implantation in (111) HgCdTe at room temperature

Myriam H. Aguirre, Horacio R. Cánepa,[a] and Noemí E. Walsöe de Reca
Programa de Investigación en Sólidos (PRINSO)-CONICET-CITEFA, San Juan Bautista de La Salle 4397, B1603ALO, Villa Martelli, Buenos Aires, Argentina

(Received 28 January 2002; accepted 8 August 2002)

HgCdTe (MCT) is an important semiconductor material used for infrared photovoltaic detectors. Although ion implantation is a widely used technique in the manufacture of devices based on MCT to obtain n/p junctions, a detailed understanding of the *n*-type behavior of the unannealed damage region has not yet been established. In this work, n/p junctions were formed by Ar^{++} implantation on MCT (111) grown by the isothermal vapor phase epitaxy method. Structural damage after implantation for different implantation doses (10^{13}, 10^{14}, and 10^{15} Ar^{++}/cm^2) was evaluated by transmission electron microscopy. At high doses, damage distribution exhibits a double region of defects. These were mainly vacancy dislocation loops and lines in the first region, whereas the second zone exhibited small dislocation loops. The observed *n*-type behavior after implantation was attributed to the generation and diffusion of Hg from the damaged region. © *2002 American Institute of Physics.* [DOI: 10.1063/1.1512695]

INTRODUCTION

The semiconductor $Hg_{1-x}Cd_xTe$ (MCT) is widely used in infrared detector technology for imaging arrays in both scanning and staring configurations. The energy gap of this material is a function of Cd concentration (x).[1] Advanced arrays of $Hg_{1-x}Cd_xTe$ require an implantation technique capable of a precise control for semiconductor junction formation. Implantation typically causes a lattice disorder as induced by defect formation which, in turn, influences structural and electrical characteristics.[2–4]

A common way to form n/p junctions in MCT-based photovoltaic devices is ion implantation. Unlike conventional implantation, the electrical activity of the implanted ion is not the most important factor.[4] The purpose of implanting is to create a source of mobile Hg interstitials. These interstitials diffuse into the material and annihilate Hg vacancies (single or double acceptors) that are present in large concentrations in *p*-type MCT grown at high temperature. If the acceptor concentration falls below that of donors, the region is converted to *n*-type.[5]

In this work, Ar^{++} implantation was on *p*-type $Hg_{1-x}Cd_xTe$, at a composition between 0.16 and 0.22, with implantation doses ranging from 10^{13} to 10^{15} Ar^{++}/cm^2. The defect generation was characterized by transmission electron microscopy (TEM) in planar view and cross section geometries.

EXPERIMENTAL PROCEDURE

Undoped *p*-type MCT was grown onto (111) CdTe substrates at PRINSO, using the isothermal vapor phase epitaxy (ISOVPE) method.[6] The eV Products Division provided the (111) CdTe substrates. Prior to growth, the substrates were chemically polished with a 2% bromine-methanol solution.

Ar^{++} was implanted at room temperature, with energies between 200 and 300 keV, doses between 10^{13} to 10^{15} Ar^{++}/cm^2, and ion current densities lower than 1.0 $\mu A/cm^2$. Table I summarizes the specimen stoichiometry and implantation conditions. All samples showed *p*-type conduction before implantation and *n*-type conduction after implantation. Specimens for TEM were thinned by a precision ion polishing system, Gatan 691 model, operated at very low voltage ($V^{+}_{Ar} < 4$ kV). The samples were examined in a JEOL 2000 FX electron microscope, equipped with a LaB_6 emitter and operating at 200 kV. An energy dispersive spectrometer (Link Pentafet 5947 Model, Oxford Microanalysis Group) was employed to analyze the chemical composition of material during TEM observations. Hall measurements by the Van der Pauw method were performed at liquid nitrogen temperature. Sheet electron concentrations were calculated by Petritz's double layer model.[7]

RESULTS

TEM analysis of implanted samples exhibited dislocation loops in every case. A few dislocation lines were observed at high doses. Loops with increasing diameter were observed by increasing doses from 10^{13} to 10^{15} Ar^{++}/cm^2. This fact was corroborated by comparison of micrographs for implanted samples (Figs. 1–4), in both types of geometry, planar view, and cross section. The evolution of loop diameter is summarized in Table II.

For the lowest doses (10^{13} Ar^{++}/cm^2), the loop diameters were small, ranging from 90 to 500 Å[Fig. 1(a)]. For doses of 10^{14} Ar^{++}/cm^2, the loop diameters were in the range of 100 to 1300 Å (with an average size of $D = 800$ Å). Also at these doses, some dislocation loops joining into larger loops or irregular dislocation lines were observed [Fig. 2(a)]. Loops with $\mathbf{b} = \frac{1}{2}\{110\}$ were observed with perfect dislocations, whereas partial Frank loops were not detected.

[a]Electronic address: canepa@citefa.gov.ar

TABLE I. Description of specimen and implantation conditions, *p*-type measurements before implantation and *n*-type measurements after implantation.

Specimen	x	Doses (Ar^{++}/cm^2)	Energy (keV)	Hg loss %	Bulk carrier density p (cm^{-3})	Sheet electron density n (cm^{-2})
VPE 91 A	0.16~0.17	10^{13}	200	6	2.03×10^{17}	7.15×10^{13}
VPE 89	0.16~0.17	10^{14}	200	5	7.46×10^{17}	4.08×10^{14}
VPE 91 B	0.16~0.17	10^{15}	200	9	2.03×10^{17}	1.01×10^{14}
VPE 40	0.22	10^{15}	300	8	1.11×10^{17}	2.15×10^{14}

For doses of 10^{15} Ar^{++}/cm^2, at implantation energies of 200 and 300 keV [Figs. 3(a) and 4(a)] the loops overlap, increasing their diameters. Loop interaction generates entanglement of the dislocation lines. Differences in dislocation shape were not observed for two different implantation energies.

Studying the samples in the cross-section geometry shows that the damaged region also changes with implanta-

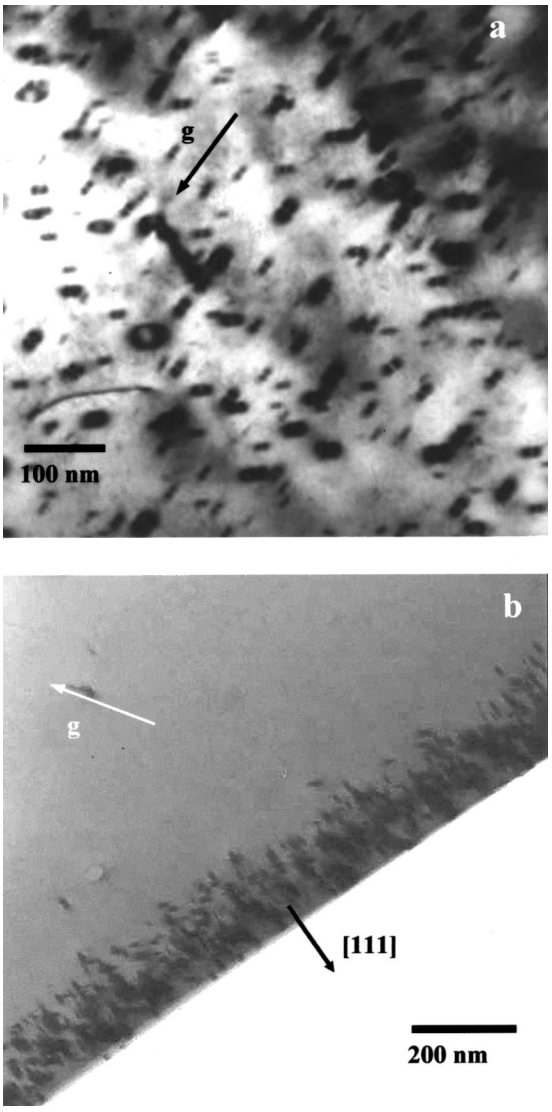

FIG. 1. VPE 91 (111) A specimen implanted with 10^{13} Ar^{++}/cm^2 at 200 keV (a) Planar view, axis zone ~ [111] and $g=[0\bar{2}\bar{2}]$. (b) Cross section, axis zone~$[\bar{1}10]$ and $\mathbf{g}=-[220]$.

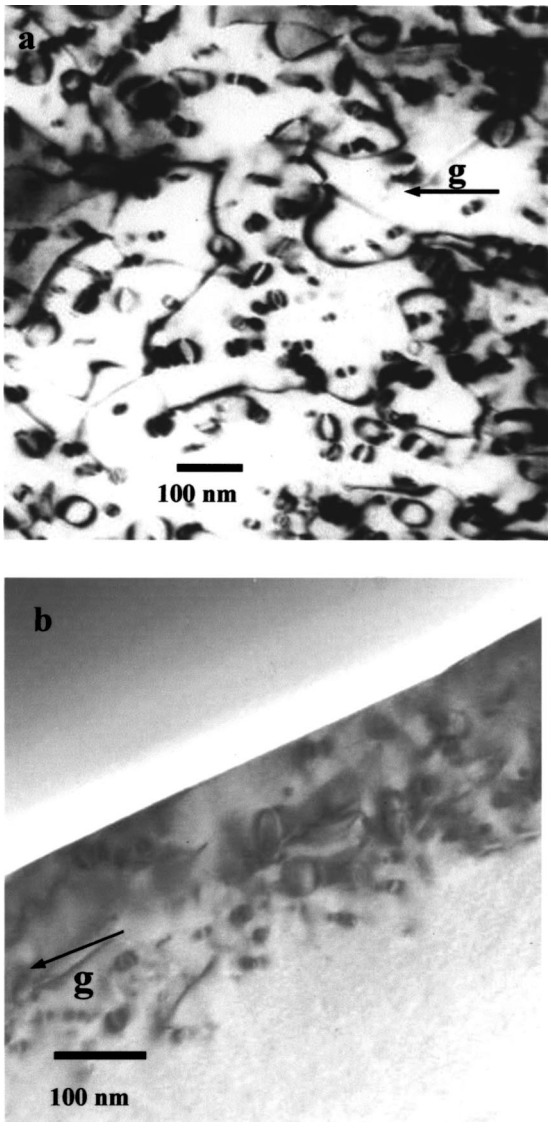

FIG. 2. VPE 89 (111) specimen implanted with 10^{14} Ar^{++}/cm^2 at 200 keV. a) Planar view, axis zone [111] and $\mathbf{g}=[0\bar{2}\bar{2}]$. (b) Cross section, axis zone~$[11\bar{2}]$ and $\mathbf{g}\approx[2\bar{2}0]$.

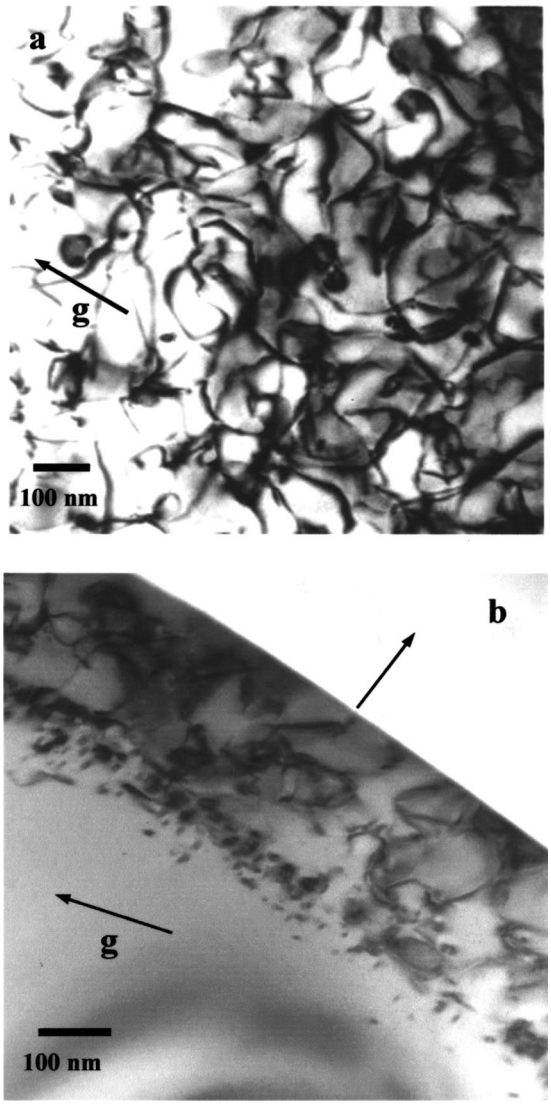

FIG. 3. VPE 91 (111) B specimen implanted with 10^{15} Ar^{++}/cm^2 at 200 keV. (a) Planar view, axis zone [111] and $\mathbf{g}\sim[\bar{2}02]$. (b) Cross section, axis zone $[1\bar{1}0]$ and $\mathbf{g}\approx[\bar{1}\bar{1}1]$.

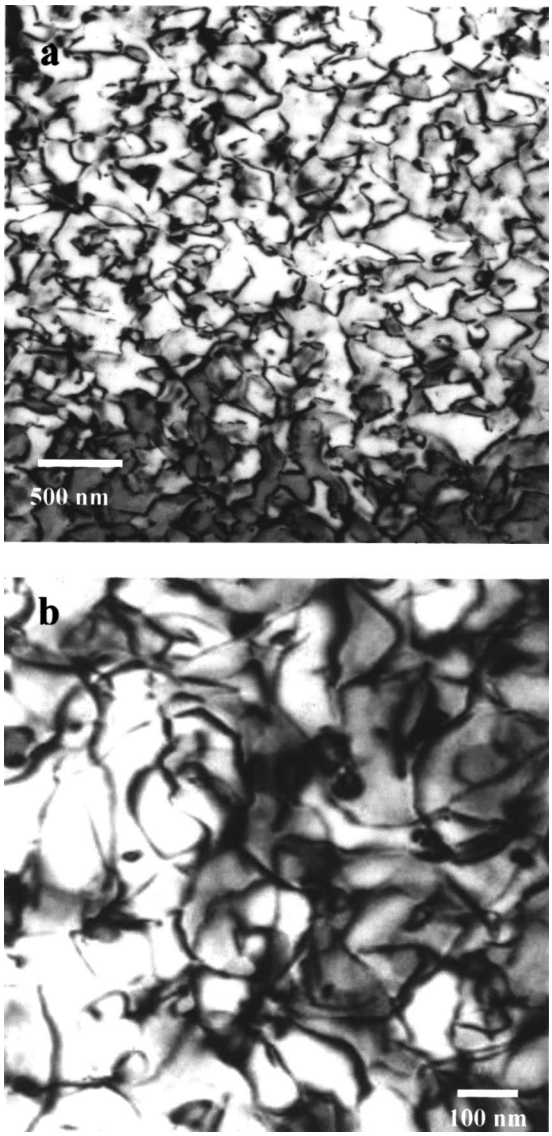

FIG. 4. VPE 40 (111) specimen implanted with 10^{15} Ar^{++}/cm^2 at 300 keV. Micrographs are on planar view, axis zone [111].

tion dose, with an increase in damage size as the dose is increased. Fig. 1(b), shows that for a specimen implanted at the lowest dose (10^{13} Ar^{++}/cm^2), a single uniform damaged region is visible. This was not the case for higher implantation doses under TEM observation.

For samples implanted at 10^{14} Ar^{++}/cm^2, a double defect region appears. The first one is formed by large dislocation loops and lines, whereas the second exhibits small dislocation loops. This double defect distribution was easily observed in samples implanted at 10^{15} Ar^{++}/cm^2 [Fig. 3(b)]. Also, at the highest implantation doses, a thin surface region (0–500 Å) was also observed, exhibiting a low defect density or no defects at all.

DISCUSSION

Defect distribution was quite different for low and high implantation doses. At low doses (10^{13} Ar^{++}/cm^2) the TEM observation exhibits a region of uniformly distributed defects (small dislocation loops). At higher doses ($\geqslant 10^{14}$ Ar^{++}/cm^2), implantation produced a double zone of defect distribution. The first region could be attributed to vacancy dislocation loops and lines coexisting with a thin surface subregion with a very low defect density or with no defects. The second region is predominantly formed of interstitial dislocation loops. These results were corroborated by TEM internal–external contrast method.

TABLE II. Loop size and damaged region size as a function of implantation doses.

Doses Ar^{++}/cm^2 200 keV	Loop Diameter		Damaged Region Cross Section (Å)
	Planar View (Å)	Cross Section (Å)	
10^{13}	90–500	80–175	$[0-1800]\pm 200$
10^{14}	120–1300	190–500	$[0-2500]\pm 200$
10^{15}	1000–2000	500–1125 (80–250)	$[0-3400]\pm 200$

TABLE III. Atomic percent of MCT components as a function of depth in cross sectional analysis by EDS in TEM *in situ* observations, Δat. % = ± 1.5 and $\Delta r = \pm 250$ Å.

At. %	0–1450 Å	1450–3000 Å	3000–4850 Å	4850–6000 Å
Cd	9.94	10.59	7.55	10.90
Te	54.40	53.61	54.42	54.63
Hg	35.65	35.80	38.03	34.47

A possible explanation for this defect distribution could be at high implantation, a high density of Hg interstitials is generated, diffusing deeply into the crystal and leaving Hg vacancies (and Cd vacancies in a lesser quantity) at the surface, which collapsed into vacancy dislocation loops and lines. This fact was corroborated by mono-energetic positron beam measurements by Uedono *et al.*[8] and by TRIM calculations[9] that showed a vacancy distribution around 0–2000 Å.

Table I reports a decreasing Hg percentage at increasing implantation doses in the region of 0–2000 Å in planar view analysis. Table III reports the Hg variation in terms of depth in cross-section analysis.

The sub-region at the surface with a few defects could be attributed to the annealing effect produced by implantation. It is known that implantation makes the temperature rise at the impinged surface.[10] In spite of testing the sample temperature during the implantation process, and the fact that a highest average value of 50°C was not reported, the local temperature at the surface may reach considerably higher values than this. This temperature can not be precisely measured. This effect may be considered similar to a recovery annealing of the crystal structure in the first region (0–500 Å).

The second region of defects is formed by small dislocation loops. The main character of these loops is interstitial and they are formed by Hg interstitial saturation (and in less quantity by Cd interstitial). These Hg interstitial atoms are generated and pushed by diffusion during the implantation process. This fact was observed in Al-implanted samples by Lévêque *et al.*[11] In their studies they have detected interstitial dislocation loops at depths between 2000 and 5000 Å using diffuse x-ray scattering measurements.

To conclude, it should be noted that the defect model described in this work is consistent with the junction model proposed by Williams *et al.*[5]

CONCLUSION

Structural damage in Ar-implanted epitaxially grown MCT has been described. TEM observations corroborates that the predominant defects produced by implantation are dislocation loops, identified in the first region of defects as vacancy-type. Loop diameter increases proportionally to implantation dose. The second defect region is formed by interstitial dislocation loops.

The *n*-type behavior observed after implantation could be attributed to generation and diffusion of Hg during implantation from the damaged region inside the crystal. Hg interstitials annihilate Hg vacancies and the conduction type conversion ensues when the donor concentration results higher than the acceptor density. The junction extends much deeper into the crystal, compared the doped layer[12] due to Hg diffusion.

ACKNOWLEDGMENTS

The authors are indebted to Dr. A. Filevich for the specimen implantation at Tandar Lab (CNEA-Argentina) and to Professor M. Á. Alario-Franco for providing facilities at the Microscopy Center ''Luis Brú'' at the Universidad Complutense, Madrid (Spain). This study was founded by CONICET Grant No. 403/97.

[1] J. Brice and P. Capper, *Properties of Mercury Cadmiun Telluride* (INSPEC, Institute of Electrical Engineering, London, 1987).
[2] L. O. Bubulac, W. E. Tennant, R. A. Riedel, and T. J. Magee, J. Vac. Sci. Technol. **21**, 251 (1982).
[3] H. F. Schaake, J. Vac. Sci. Technol. A **4**, 2174 (1986).
[4] G. L. Destefanis, J. Cryst. Growth **86**, 700 (1988).
[5] B. Williams, H. Robinson, and C. Helms, J. Electron. Mater. **27**, 538 (1998).
[6] J. G. Fleming and D. A. Stevenson, J. Cryst. Growth **82**, 621 (1987).
[7] R. L. Petritz, Phys. Rev. **110**, 1254 (1958).
[8] A. Uedono, H. Ebe, M. Tanaka, R. Suzuki, T. Ohdaira, S. Tanigawa, T. Mikado, K. Yamamoto, and Y. Miyamoto, Jpn. J. Appl. Phys. **37**, 3910 (1998).
[9] J. Ziegler, TRIM95, IBM Corp. (1995).
[10] Cécile Uzan, Doctoral thesis, University of Paris VII, 1986.
[11] P. Lévêque, A. Declémy, and P. O. Renault, Nucl. Instrum. Methods Phys. Res. B **168**, 40 (2000).
[12] L. Bubulac, W. Tennant, R. Riedel, and T. Magee J. Vac. Sci. Technol. **21**, 253 (1982).